

Supplementary information

Vapor selective and controlled actuation of gelatin-based soft actuator

Vipin Kumar^{a,b}, Sarah Ahmad Siraj^{a,b}, Dillip K. Satapathy*^{a,b}

^aSoft Materials Laboratory, Department of Physics, IIT Madras, Chennai, India

^bCenter for Soft and Biological Matter, IIT Madras, Chennai-600036, Tamil Nadu, India

E-mail: dks@iitm.ac.in

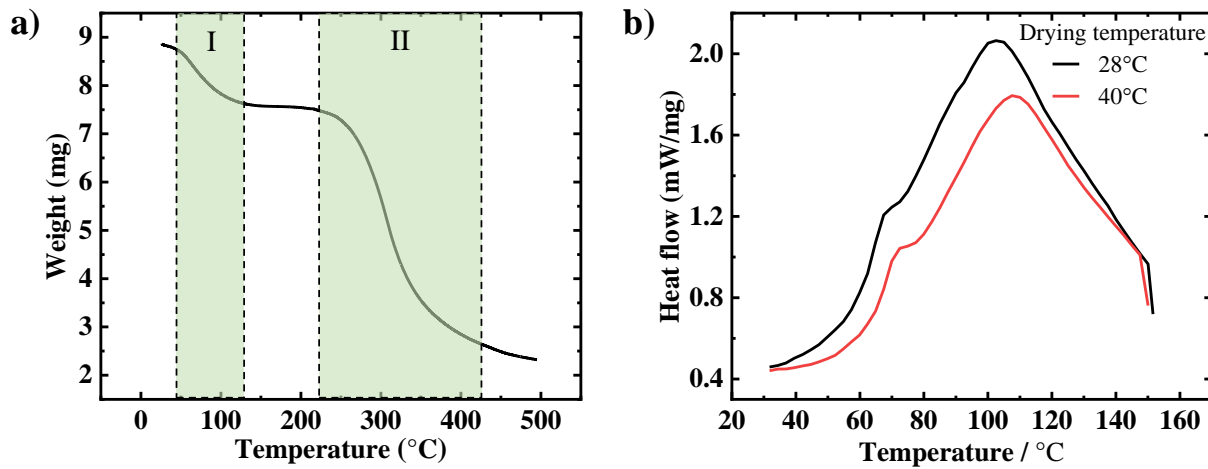


Figure S1: (a) Thermogravimetric analysis (TGA) plot provides the weight loss measured as a function of temperature. The plot shows two stages of weight loss in the gelatin film; the first stage corresponds to the evaporation of the free and bound water, and the second stage corresponds to the thermal degradation of the proteins inside the gelatin film. (b) Differential scanning calorimetry (DSC) plot of the gelatin films dried at 28 °C (black curve) and 40 °C (red curve) shows two transition peaks; the first peak (68 °C-71 °C) corresponds to the glass to rubber transition, and the second peak (102 °C-107 °C) corresponds to the melting of the gelatin film.

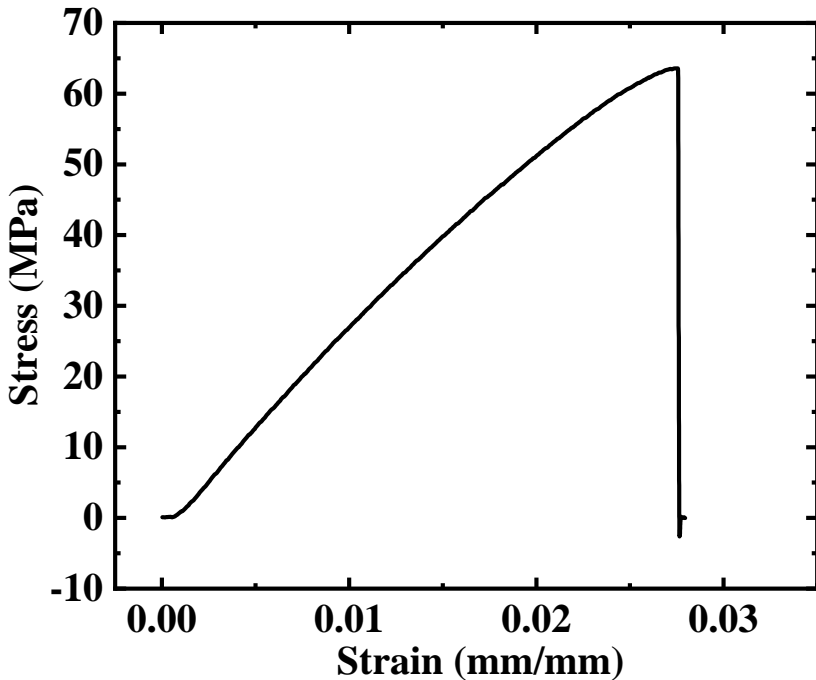


Figure S2: Stress-strain curve of the gelatin film with the extension rate of 2 mm/min. The measurement was performed at room temperature = 25 °C and relative humidity = 45% with the gauge length = 30 mm, width = 12 mm, and thickness = $23 \pm 1 \mu\text{m}$.

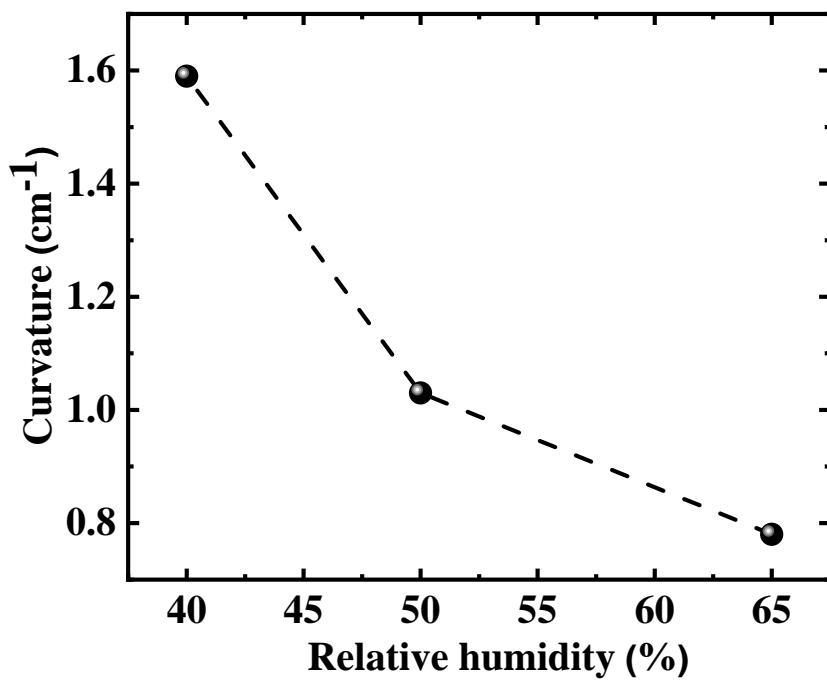


Figure S3: The maximum bending curvature of the gelatin film upon exposure to the water vapor in different relative humidities. The curvature decreases as the relative humidity in the environment increases. This decrease in curvature is due to a decrease in the strain gradient along the thickness of the film at higher relative humidities. Dimensions of the film: $l = 16 \text{ mm}$, $w = 16 \text{ mm}$ and $t = 15 \mu\text{m}$.

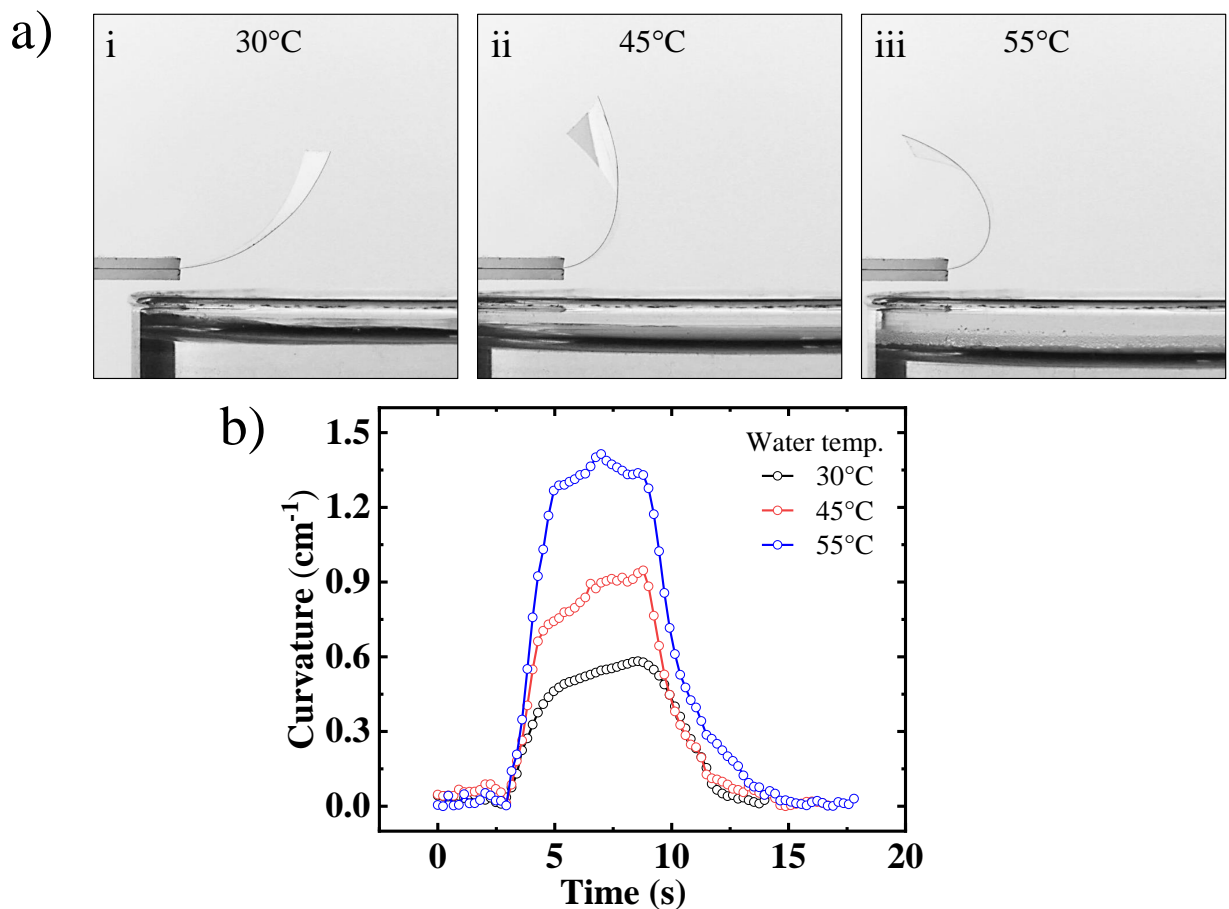


Figure S4: (a) Snapshots of the maximum bending state of the gelatin film upon exposure to the water vapor coming from the source maintained at three different temperatures: i-30°C, ii- 45°C and iii-55°C. (b) The time evolution of maximum bending curvature of the actuator upon exposure to the water vapor coming from the source is maintained at three different temperatures (30°C, 45°C, and 55°C).

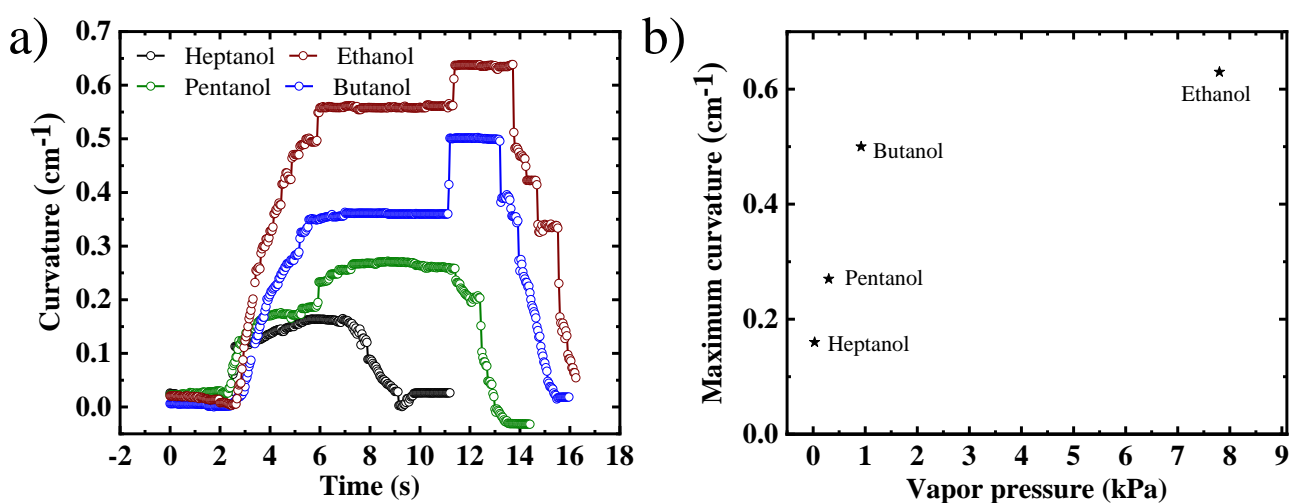


Figure S5: (a) The temporal evolution of bending curvature of the gelatin film upon exposure to different organic solvent vapors. (b) The maximum bending curvature value of the gelatin film as a function of vapor pressure of respective solvents.

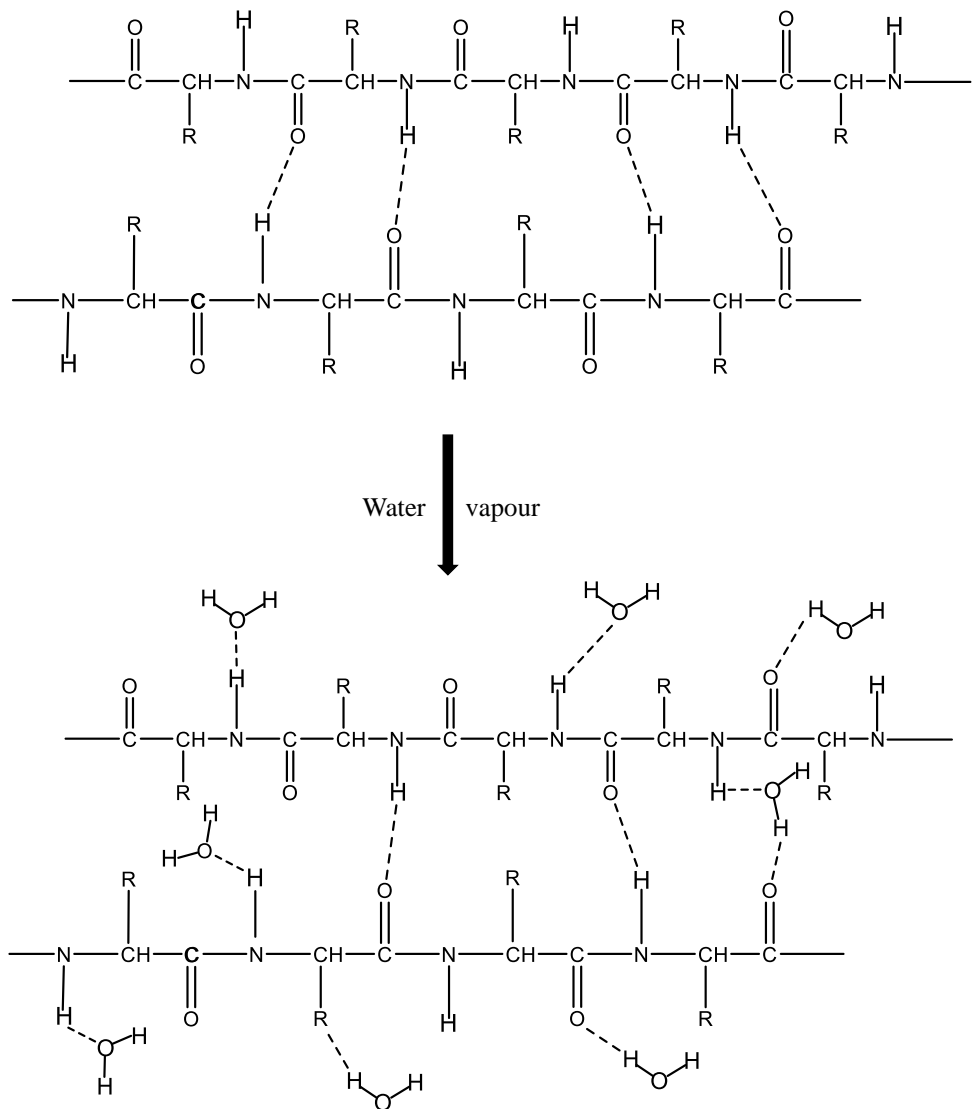


Figure S6: The molecular structure of the gelatin before (upper panel) and after the water vapor exposure. It can be seen that the protein chains are interconnected via hydrogen bonds, and few hydrophilic groups are free to absorb the water vapor (upper panel). Upon exposure to the water vapor, these free hydrophilic groups interact and absorb water molecules, which facilitates the swelling of the gelatin film. The hydrogen bonds between the chains may also break in the presence of water vapor to absorb the water molecules.

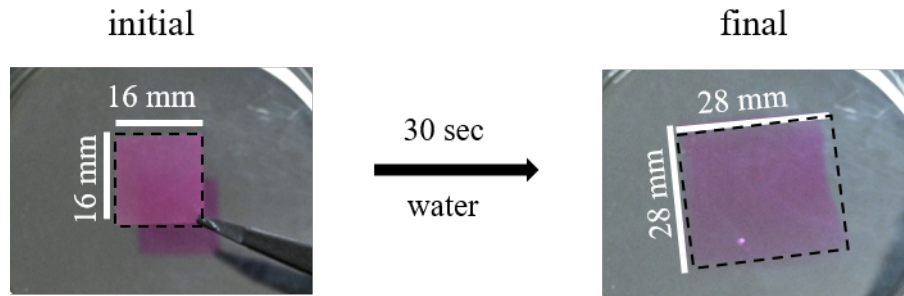


Figure S7: Sanpshots of the gelatin film before and after dipping into the liquid water. The length and width of the gelatin film increase from 16 to 28 mm within 30 seconds due to water absorption by the gelatin film.

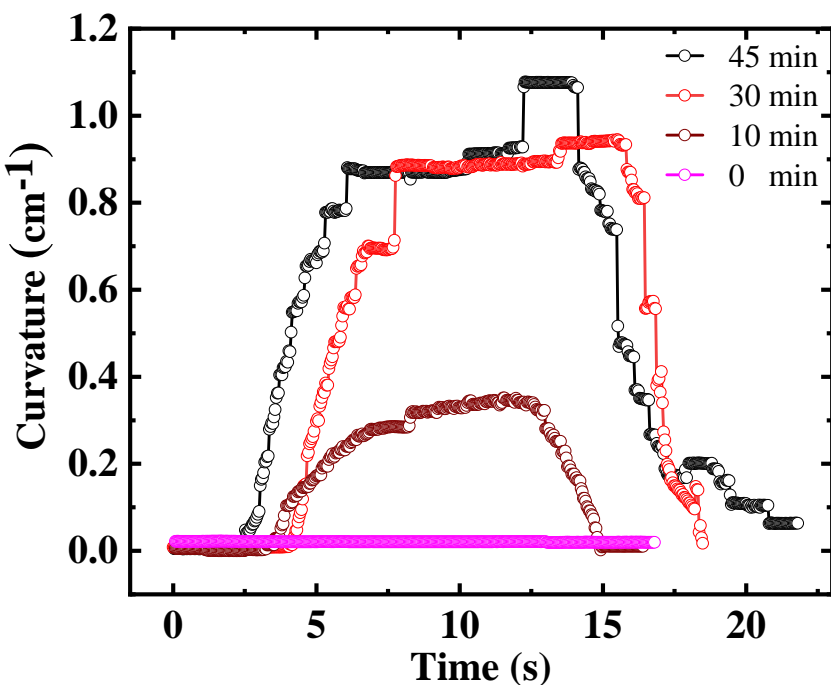


Figure S8: The temporal evolution of the bending curvature of gelatin film upon exposure to dehydrated silica gel with different dehydration times at a fixed temperature 100 °C on the hot plate. The atmospheric humidity was kept constant at 70% during the experiment. Dimensions of the film: $l = 30$ mm, $w = 25$ mm, and $t = 30 \pm 1 \mu\text{m}$.

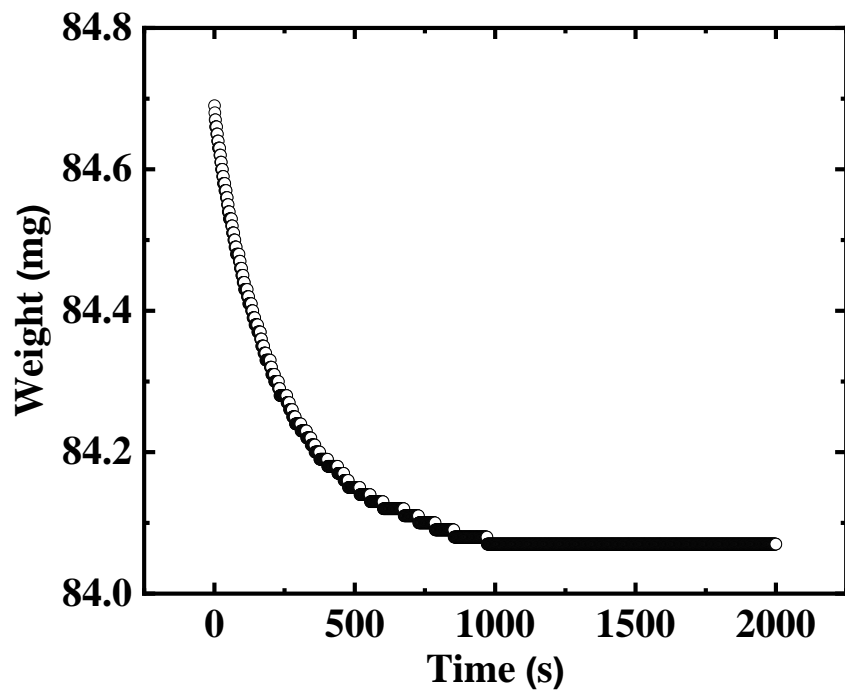


Figure S9: The weight change of the gelatin film in ethanol vapor environment.

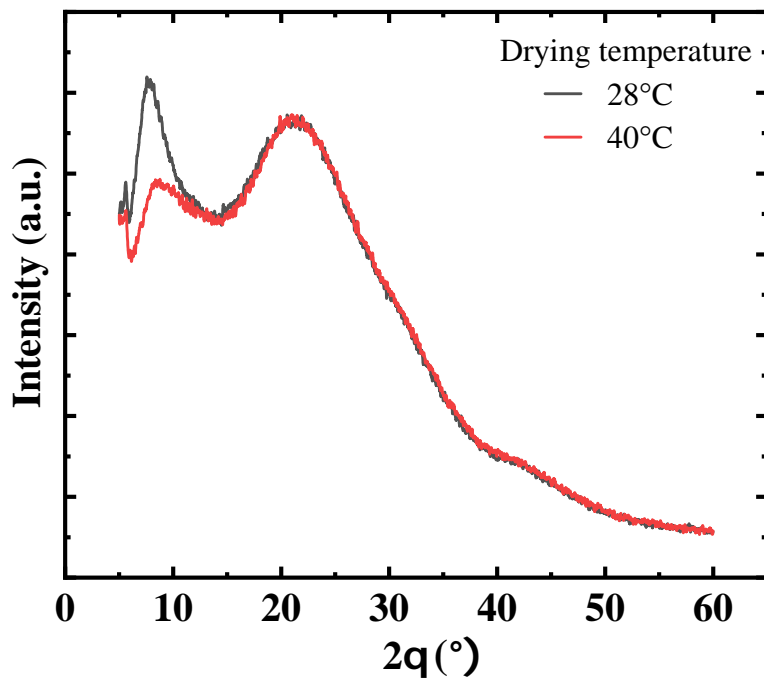


Figure S10: X-ray diffraction pattern recorded for the gelatin films dried at 28 ± 1 °C and 40 ± 1 °C. It was noticed that, as the drying temperature increases from 28 °C to 40 °C, the amount of triple helix decreases due to a decrease in the peak intensity at $2\theta = 7^\circ$ corresponding to the triple helix content in the film.

Table S1: Table of partial pressure of water and ethanol in the mixture and corresponding bending curvature.

Water (%) in the mixture	Partial pressure of water (kPa)	Partial pressure of ethanol (kPa)	Actuation direction	Curvature (cm^{-1})
100	3.17	0	upward	0.71
80	2.94	0.56	upward	0.69
40	2.17	2.48	upward	0.61
20	1.42	4.34	none	0
10	0.84	5.78	downward	0.43
0	0	7.86	downward	0.58

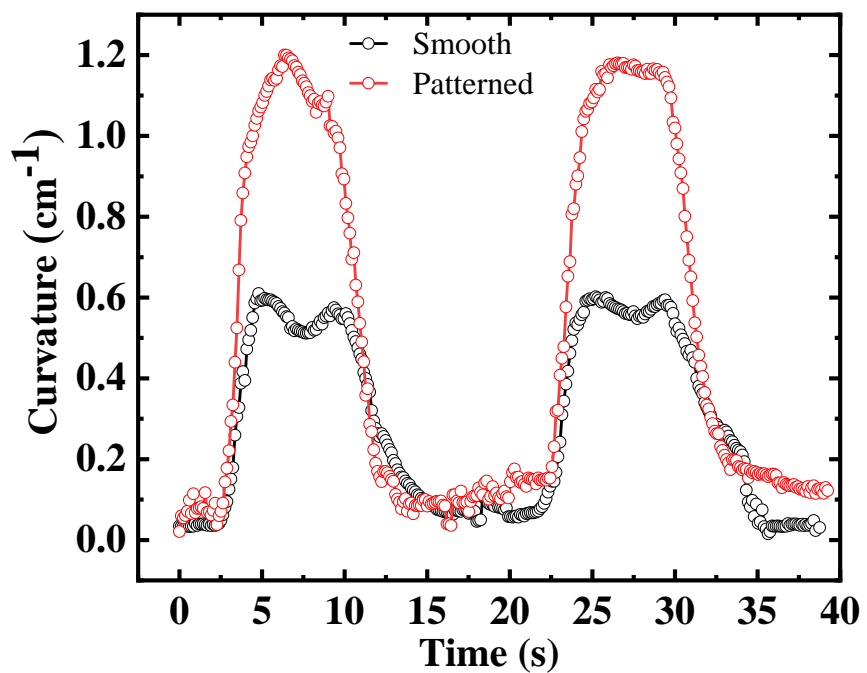


Figure S11: The temporal evolution of bending curvature of smooth (black) and patterned (red) film. The bending rate and curvature of the patterned film are higher than smooth film.

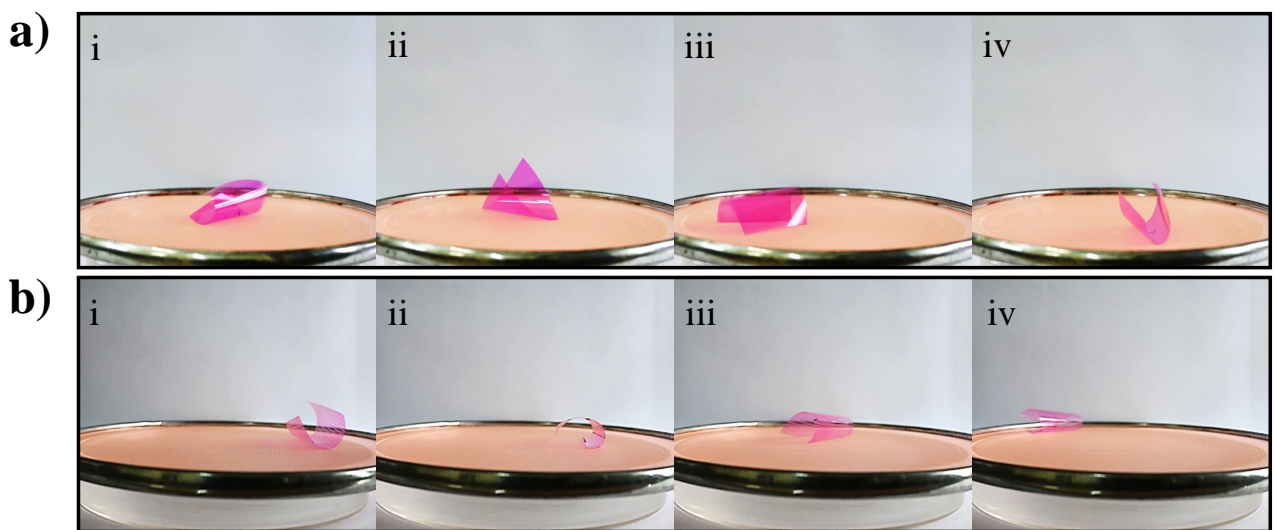


Figure S12: (a) Snapshots of the square-shaped non-patterned gelatin film at different times while doing locomotion upon exposure to the water vapor from the bottom side. The dimensions of the film: $l = 4 \text{ cm}$, $w = 4 \text{ cm}$, and $t = 18 \pm 3 \mu\text{m}$. (b) Snapshots of the square-shaped patterned gelatin film at different times while doing linear motion upon exposure to the water vapor from the bottom side. The dimensions of the film: $l = 4 \text{ cm}$, $w = 4 \text{ cm}$, and $t = 22 \pm 5 \mu\text{m}$.

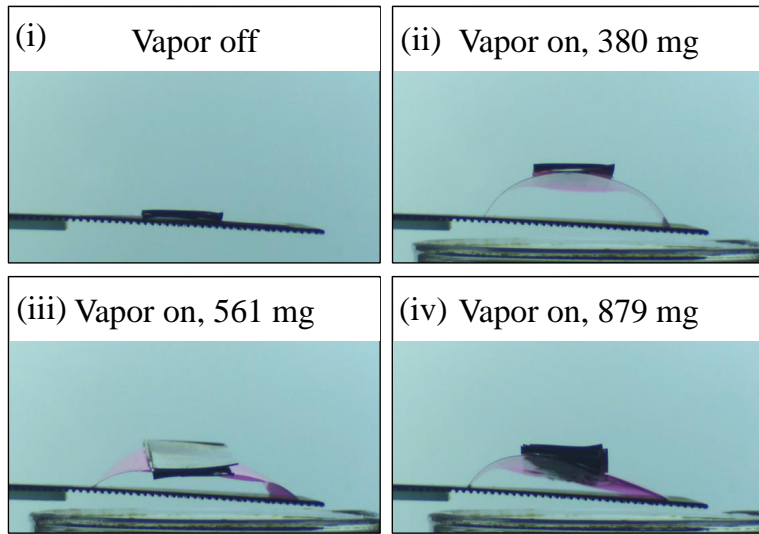


Figure S13: (i) Snapshot of the gelatin film with attached weight in its initial flat state in the absence of ethanol vapor. (ii), (iii), and (iv) Snapshot of the gelatin film with attached weight in the presence of ethanol vapor on the bottom side. We note that as the weight attached to the gelatin film increases, the lifting height decreases.

Table S2: Comparison table of gelatin and non-gelatin based vapor responsive soft actuators

System	Materials	Biodegradable/ Biocompatible	Stimuli	Actuation speed	Repeatability	Bidirectional/ Control	Ref.
Gelatin based soft actuators	Gelatin + PEDOT:PSS	No/Yes	Water vapor	NA	NA	No/No	[1]
	Gelatin soaked in tannic acid	Yes/Yes	Temperature	NA	NA	No/Yes	[2]
	Gelatin bilayers	Yes/Yes	Water	recovery time 1s	NA	No/Yes	[3]
	Gelatin bilayers	Yes/Yes	Water, pH	slow	NA	No/Yes	[4]
Non- gelatin based soft actuators	Pollen	Yes/Yes	Water vapour	0.02 $\text{cm}^{-1}\text{s}^{-1}$	NA	No/No	[5]
	Cellulose nanofibers	Yes/Yes	Water vapour	0.01 $\text{cm}^{-1}\text{s}^{-1}$	20 cycles	No/No	[6]
	Silk fibroin	Yes/Yes	Water vapour	53.19 $\text{cm}^{-1}\text{s}^{-1}$	1000 cycles	No/No	[7]
	Graphene oxide	No/No	Water vapour	30° s^{-1}	10 cycles	No/No	[8]
	MXene	No/No	Water vapour	8° s^{-1}	10 cycles	No/No	[9]
	GO+MXene with Bacterial cellulose	No/No	Water vapour	29° s^{-1}	20 cycles	No/No	[10]
	Dried bonito film	Yes/Yes	Water vapour	40° s^{-1}	NA	No/No	[11]
	Gelatin	Yes/Yes	Water and alcohol vapors	1 $\text{cm}^{-1}\text{s}^{-1}$	1200 cycles	Yes/Yes	This work
	without additives						

Movie S1: The bending and unbending of the gelatin film in the exposure and withdrawal of the water vapor for a single cycle

Movie S2: Effect of the drying temperature on the actuation

Movie S3: Effect of the post-annealing on the actuation

Movie S4: Film with patterns orientated in different directions upon exposure to water vapor

Movie S5: Actuation performance of smooth and patterned surface gelatin film

Movie S6: Locomotion and linear motion of circular-shaped film

Movie S7: Locomotion and linear motion of square-shaped film

Movie S8: Gelatin film as an ethanol vapor sensor

Movie S9: Gelatin film as humidity-gated smart curtains

Movie S10: Gelatin film as smart lift

Movie S11: Wave-like structure of the gelatin film upon exposure to water and ethanol vapors in a sequential manner

Movie S12: Voltage generation (water vapor to voltage generation)

References

- (1) Liu, Y.; Sun, X.-C.; Lv, C.; Xia, H. *Smart Materials and Structures* **2021**, *30*, 125014.
- (2) Yang, S.; Zhang, Y.; Wang, T.; Sun, W.; Tong, Z. *ACS Applied Materials & Interfaces* **2020**, *12*, 46701–46709.
- (3) Hanzly, L. E.; Kristofferson, K. A.; Chauhan, N.; Barone, J. R. *Green Materials* **2021**, *9*, 157–166.
- (4) Riedel, S.; Heyart, B.; Apel, K. S.; Mayr, S. G. *Scientific Reports* **2017**, *7*, 17436.
- (5) Zhao, Z.; Hwang, Y.; Yang, Y.; Fan, T.; Song, J.; Suresh, S.; Cho, N.-J. *Proceedings of the National Academy of Sciences* **2020**, *117*, 8711–8718.
- (6) Wang, M.; Tian, X.; Ras, R. H.; Ikkala, O. *Advanced Materials Interfaces* **2015**, *2*, 1500080.
- (7) Manikandan, G.; Murali, A.; Kumar, R.; Satapathy, D. K. *ACS Applied Materials & Interfaces* **2021**, *13*, 8880–8888.
- (8) Ge, Y.; Cao, R.; Ye, S.; Chen, Z.; Zhu, Z.; Tu, Y.; Ge, D.; Yang, X. *Chemical Communications* **2018**, *54*, 3126–3129.
- (9) Wang, J.; Liu, Y.; Cheng, Z.; Xie, Z.; Yin, L.; Wang, W.; Song, Y.; Zhang, H.; Wang, Y.; Fan, Z. *Angewandte Chemie International Edition* **2020**, *59*, 14029–14033.
- (10) Ge, Y.; Zeng, J.; Hu, B.; Yang, D.-Y.; Shao, Y.; Lu, H. *Giant* **2022**, *11*, 100107.

- (11) Chen, Z.; Peng, Q.; Hu, Y.; Liu, Z.; Zhao, X.; Li, P.; Xu, L.; Zheng, H.; Xue, F.; Ding, R., et al. *Journal of Materials Science & Technology* **2023**, *167*, 152–160.